Journal of Wind Engineering & Industrial Aerodynamics 177 (2018) 60–68

Contents lists available at ScienceDirect

Journal of Wind Engineering & Industrial Aerodynamics

journal homepage: www.elsevier.com/locate/jweia

A numerical study of the aerodynamic characteristics of ice-accreted transmission lines

Takeshi Ishihara [a,*], Shinichi Oka [b]

[a] Department of Civil Engineering, School of Engineering, The University of Tokyo, 7-3-1 Hongo, Bunkyo-ku, Tokyo 113-8656, Japan
[b] NUMECA Japan Co., Ltd., Kitamura Bldg., 1-17-15, Nishi-shinbashi, Minato-ku, Tokyo 105-0003, Japan

ARTICLE INFO

Keywords:
LES
Aerodynamic coefficients
Ice heights effect
Wake effect
Correction coefficient

ABSTRACT

Aerodynamic coefficients of single and 4-bundled ice-accreted conductors are investigated using the LES turbulence model and compared with the results of the wind tunnel test. Single conductors with span lengths of $L = 1D$ and $10D$ are simulated, and the predicted aerodynamic coefficients with a span length of $L = 10D$ show good agreement with the measured those within the estimated error range of the wind tunnel test, where D is the diameter of the single conductor. A systematic error estimation using the models with $L = 2D$, $3D$, and $6D$ is conducted; the results show that a span length of $L = 10D$ is long enough to predict aerodynamic coefficients. The effect of the accreted ice height, H, on the aerodynamic coefficients is investigated. It is found that negative pressure at the lower face near the leading edge significantly affects C_L and C_M and leads to the maximum absolute values of C_L and C_M at 12° for the conductor with $H = 1D$ and at 16° for the conductor with $H = 0.5D$. The wake effect of 4-bundled conductors is also investigated by the analysis of the aerodynamic coefficients and the pressure distribution for each conductor. The wake of the windward conductors has a significant impact on C_L and C_M. Correction coefficients for leeward conductors are proposed to account for the wake effect, and the results show good agreement with the predicted aerodynamic coefficients of the 4-bundled conductors.

1. Introduction

Large-amplitude wind-induced vibrations of ice-accreted transmission lines, called galloping, a form of single-degree-of-freedom aerodynamic instability, which can occur for long bodies with certain cross-sections (Holmes, 2001), could cause inter-phase short circuits or damage to insulators and support structures; in the worst case, such damage results in the shutdown of a transmission line (Scanlan, 1972). Hence, it is important to understand and evaluate the galloping phenomenon to establish countermeasures to prevent an accident. Many studies have reported the assessment of the galloping phenomenon (Den Hartog, 1956; Parkinson, 1971; Novak, 1972; Cooper, 1973; Kimura et al., 1999; Matsumiya and Nishihara, 2012). In a galloping evaluation, numerical analysis based on a quasi-steady approach is widely used in which the aerodynamic coefficients are obtained first and then response analysis is performed to evaluate the amplitude of vibrations. Software has been developed to predict the response of a transmission line. For example, Shimizu and Sato (2001) developed a finite element analysis code that accounts for the geometrical non-linearity of a transmission line, by which galloping simulations and analysis of the vibration characteristics are conducted. In general, aerodynamic coefficients are required for input data in such code. It is possible to obtain aerodynamic coefficients of ice-accreted transmission lines using a wind tunnel test (Shimizu et al., 2004; Matsumiya et al., 2010). However, a wind tunnel test is time consuming and costly because of the need to create a new model every time for each test. The aerodynamic coefficients of each sub-conductor must be obtained to predict the galloping of 4-bundled conductors accurately (Matsumiya and Nishihara, 2013). Shimizu et al. (2004) proposed a method to convert the aerodynamic coefficients of a single conductor into those of 4-bundled conductors; the results were in good agreement with those for the 4-bundled conductor by the wind tunnel test with regard to C_D and C_L, but a discrepancy was observed in C_M because the wake effect was not taken into account in the method. Matsumiya et al. (2010) clarified the wake effects of windward conductors on the leeward conductors using pressure measurements for all of the sub-conductors. However, in contrast to the force balance test, it is difficult to create models with pressure measurement probes. In addition, the locations and the number of measurement points are sensitive to the results.

Recently, numerical analysis has become a popular method for

* Corresponding author.
E-mail address: ishihara@bridge.t.u-tokyo.ac.jp (T. Ishihara).

https://doi.org/10.1016/j.jweia.2018.04.008
Received 28 August 2017; Received in revised form 25 November 2017; Accepted 9 April 2018

obtaining aerodynamic coefficients of bluff bodies, such as circular cylinders and rectangular prisms. Oka and Ishihara (2009) used LES to predict the aerodynamic coefficients of a square prism, and they were found to be in good agreement with the wind tunnel test results. In addition, Oka and Ishihara (2010) showed that the aerodynamic coefficients of a single conductor using LES for ice-accreted transmissions lines were in good agreement with the experiments for the region of angle of attacks from 0° to 12°. However, a discrepancy was found between 16° and 20°, where the lift coefficients change substantially. In that research, correction formulas were proposed for the 4-bundled conductor model, for which the wake effects of windward conductors were taken into account, and improvements were observed in predicting C_D at angles of attack in the range from 0° to 90°; however, no results were presented for C_L or C_M.

Based on the above discussion, a numerical analysis of single-conductor transmission lines is conducted to clarify the impact of the span length on the accuracy of the aerodynamic coefficients. Firstly, the span length independent aerodynamic coefficients are evaluated to determine a span length that is sufficiently long to capture the three-dimensionality of turbulence. Next, the aerodynamic coefficients with respect to the different height of the accreted ice are investigated and effects of the height of the accreted ice on the aerodynamic characteristics are clarified by the predicted pressure distributions. Finally, the aerodynamic coefficients and pressure distributions of sub-conductors for 4-bundled conductors are investigated to show the wake effects of windward conductors on the aerodynamic coefficients of leeward conductors. In addition, correction coefficients are proposed for leeward conductors in the conversion from the single-conductor aerodynamic coefficients to the 4-bundled conductor ones to account for the wake effect.

2. Numerical model and boundary conditions

2.1. Governing equations

The governing equations for the LES model are obtained by filtering the time-dependent Navier-Stokes equations as follows:

$$\frac{\partial \rho \tilde{u}_i}{\partial x_i} = 0, \tag{1}$$

$$\frac{\partial}{\partial t}(\rho \tilde{u}_i) + \frac{\partial}{\partial x_j}(\rho \tilde{u}_i \tilde{u}_j) = \frac{\partial}{\partial x_j}\left(\mu \frac{\partial \tilde{u}_i}{\partial x_j}\right) - \frac{\partial \tilde{P}}{\partial x_i} - \frac{\partial \tau_{ij}}{\partial x_j}, \tag{2}$$

where $\tilde{u}_j$ and $\tilde{p}$ are the filtered mean velocity and the filtered pressure, respectively. ρ is the density, and τ_{ij} is the subgrid-scale stress defined by

$$\tau_{ij} = \rho \tilde{u}_i \tilde{u}_j - \rho \widetilde{u_i u_j} \tag{3}$$

The subgrid-scale stresses resulting from the filtering operations are unknown and are modeled as follows:

$$\tau_{ij} = -2\mu_t \tilde{S}_{ij} + \frac{1}{3}\tau_{kk}\delta_{ij}, \tag{4}$$

where μ_t is the subgrid-scale turbulent viscosity and $\tilde{S}_{ij}$ is the rate-of-strain tensor for the resolved scale and is defined by

$$\tilde{S}_{ij} = \frac{1}{2}\left(\frac{\partial \tilde{u}_i}{\partial x_j} + \frac{\partial \tilde{u}_j}{\partial x_i}\right). \tag{5}$$

The Smagorinsky model (Smagorinsky, 1963) is used for the subgrid-scale turbulent viscosity, μ_t.

$$\mu_t = \rho L_s^2 |\tilde{S}| = \rho L_s \sqrt{2\tilde{S}_{ij}\tilde{S}_{ij}}, \tag{6}$$

where L_s is the mixing length for subgrid-scales and is defined as

$$L_s = \min(\kappa\delta, C_s V^{1/3}). \tag{7}$$

where κ is the von Karman constant, 0.42; C_s is the Smagorinsky constant, with 0.032 used in this study (Oka and Ishihara, 2009); δ is the distance to the closest wall; and V is the volume of a computational cell.

2.2. Boundary conditions

When a wall-adjacent cell is in the laminar sublayer, the wall shear stress is obtained from the laminar stress-strain relationship as follows:

$$\frac{\tilde{u}}{u_\tau} = \frac{\rho u_\tau y}{\mu}, \tag{8}$$

If a mesh cannot resolve the laminar sublayer, then it is assumed that the centroid of the wall-adjacent cells falls within the logarithmic region of the boundary layer, and the law-of-the-wall is employed.

$$\frac{\tilde{u}}{u\tau_\tau} = \frac{1}{\kappa}\ln E\left(\frac{\rho u_\tau y}{\mu}\right). \tag{9}$$

where $\tilde{u}$ is the filtered velocity that is tangential to the wall, u_τ is the friction velocity, κ is the von Kármán constant, and the constant E has a value of 9.8. The uniform velocity condition is specified at the inlet boundary, and the zero-diffusive conditions are used at the outlet boundary. Symmetry conditions are given for both sides and for the upper/lower boundaries.

2.3. Numerical set-up

The finite volume method and the unstructured collocated mesh are used for the present simulations. The second-order central difference scheme is used for the convective and viscosity term, and the second-order implicit scheme is used for the unsteady term. The SIMPLE (Semi-Implicit Pressure Linked Equations) algorithm is employed for solving the discretized equations (Ferziger and Peric, 2002). All simulations are performed with ANSYS FLUENT.

Fig. 1 shows the cross-sectional dimensions of the ice-accreted conductor geometry models used in this study. Table 1 shows the major parameters for the analysis. Fig. 2 shows the mesh near the ice-accreted single conductor in which the diameter of the single

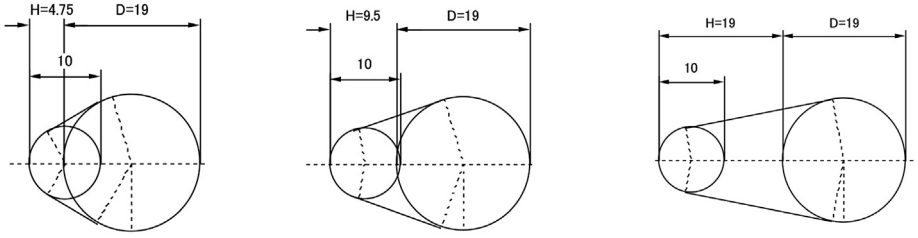

(a)) H=0.25D (b) H=0.5D (c) H=1D

Fig. 1. Cross-sectional dimensions of the conductors and the accreted ice geometry.

Table 1
Main parameters used in this study.

Conductor type	Single conductor	4-bundled conductor
Diameter D (mm)	19	
Height of the accreted ice H (mm)	$1D$, $0.5D$, $0.25D$	$1D$
Representative diameter B (mm)	19	247
Projection area A (mm^2)	38 ,100	48 ,260
Calculation domain (mm)	$60D \times 120D$	$90D \times 180D$
Span length L (mm)	$1D$, $10D$	$10D$
Grid number	465 , 50 (L=$1D$) 4 ,651 ,500 (L=$10D$)	10 ,344 ,500 (L=$10D$)
Cell size in the span direction	$0.1D$	
Non-dimensional time step size Δt	0.04	
Inflow wind velocity U (m/s)	10	
Air density ρ (kg/m^3)	1.225	
Viscosity μ (kg/ms)	1.789×10^5	
Reynolds number Re (=$\rho UD/\mu$)	13 ,007	

conductor, D, is 19 mm. The computational domain is $60D$ for the crosswind direction and $120D$ for the alongwind direction. The domain sizes of the upstream and downstream flows from the center of the conductor are set to $30D$ and $90D$, respectively. The blockages of 0° and 30° are 1.7% and 2.5%, respectively, which indicates that the blockage effect is sufficiently low. Fig. 3 shows the mesh near the ice-accreted 4-bundled conductors. The diameter of each sub-conductor, D, is 19 mm, the same as that of a single conductor. The computational domain is $60D$ for the crosswind direction and $180D$ for the alongwind direction. The domain sizes of the upstream and downstream flows from the center of the conductor are set to $60D$ and $120D$, respectively. The blockages of 0° and 30° are 2.2% and 3.3%, respectively, which indicates that the blockage effect is sufficiently low as well.

A uniform flow with a 10 m/s wind velocity is used for the inflow boundary condition. The non-diffusive condition is used for the outlet boundary condition, and the symmetry conditions are used for the side, top, and bottom walls. A set of 5 000 time step calculations is performed in which the mean aerodynamic coefficients are obtained by taking the average from the 1 000-steps data to the 5 000-steps data.

The mesh for the perimeter of the ice-accreted conductors of single conductor is divided into 150 grids. In addition, the span length, L, is set to $L = 1D$ and $10D$ for the single conductor model, and $L = 10D$ is used for the 4-bundled conductor model. Six cases, i.e., the angles of attack of 0°, 8°, 12°, 16°, 20°, and 28°, are calculated for both single and 4-bundled conductor models in this study. The Reynolds number is 13 ,007 for both single and 4-bundled conductor models in which the diameter of the sub-conductor of the 4-bundled conductor is a typical size of the wind tunnel test. The values of the Reynolds number (Shimizu et al., 2004) for the wind tunnel tests are between 1.24×10^4 and 1.95×10^4; in this range, the Reynold's effect can be ignored.

2.4. Definition of the aerodynamic coefficient and the pressure coefficient

2.4.1. Pressure coefficient

The following equation shows the definition for the pressure coefficient C_{pi} in the i-th grid on the surface of the ice-accreted conductors.

$$C_{pi} = \frac{p_i - p_{ref}}{\frac{1}{2}\rho U^2} \tag{10}$$

where p_{ref} is the reference pressure, which uses the pressure value at the center in the span direction for the bottom left corner of the inflow boundary. ρ is the air density, with a value of 1.225 kg/m^3, and U is the reference wind speed, which is the same as the inflow wind speed. The average in the spanwise direction after averaging C_{pi} over time steps ranging between 1 000 and 5 000 is used for the pressure coefficient C_p for the single conductor models. The same averaging operations are also used for the drag, lift, and moment coefficients.

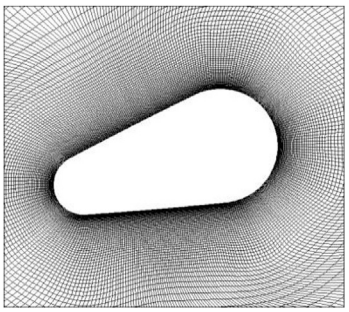

Fig. 2. Mesh near the ice-accreted single conductor.

2.4.2. Definitions of the drag, lift, and moment coefficients

Fig. 4 shows the definition of the direction for the aerodynamic coefficients and the angle of attack for the single conductor and 4-bundled conductors, which is a positive direction. The drag, lift, and moment coefficients (C_D, C_L, and C_M, respectively) for the single conductor are defined in the following equations.

$$C_D = \frac{2\sum_i F_{Di}A_i}{\rho LDU^2} \tag{11}$$

$$C_L = \frac{2\sum_i F_{Li}A_i}{\rho LDU^2} \tag{12}$$

$$C_L = \frac{2\sum_i F_{Mi}A_i}{\rho LDU^2} \tag{13}$$

where F_{Di}, F_{Li}, F_{Mi}, and A_i are the drag, lift, moment, and surface area, respectively, of the i-th grid on the ice-accreted conductor surface. L denotes the span length of the model, and B represents the reference diameter, which is 19 mm (=D) for the single conductor.

The equation for converting the aerodynamic coefficient for the single conductor into that for the 4-bundled conductors is as follows (Shimizu et al., 2004).

$$C_D^4 = \frac{1}{2}\left(C_D^{4-1} + C_D^{4-2} + C_D^{4-3} + C_D^{4-4}\right) \tag{14}$$

$$C_L^4 = \frac{1}{2}\left(C_L^{4-1} + C_L^{4-2} + C_L^{4-3} + C_L^{4-4}\right) \tag{15}$$

$$\begin{aligned} C_M^4 = {} & \frac{D}{2B}\left(C_M^{4-1} + C_M^{4-2} + C_M^{4-3} + C_M^{4-4}\right) \\ & + \frac{1}{2\sqrt{2}}\left(-C_D^{4-1} + C_L^{4-2} + C_D^{4-3} + C_L^{4-4}\right)\sin\left(\frac{\pi}{4} - \alpha\right) \\ & + \frac{1}{2\sqrt{2}}\left(-C_L^{4-1} + C_D^{4-2} + C_L^{4-3} + C_D^{4-4}\right)\cos\left(\frac{\pi}{4} - \alpha\right) \end{aligned} \tag{16}$$

where the suffix 4-1 ~ 4-4 denotes the corresponding conductors.

3. Verification of the numerical model

A sufficiently long model in the spanwise direction is necessary to capture the three-dimensionality of the turbulence flow (Rodi, 1997; Oka and Ishihara, 2010). In this section, the aerodynamic coefficients of a single-conductor transmission line is predicted for $H = 1D$ models that vary with span length. Next, the aerodynamic coefficients of the 4-bundle conductor model with the span length of $L = 10D$ are predicted to investigate the accuracy of the numerical analysis and the wind tunnel test, which was performed in the Wind Engineering Laboratory of the

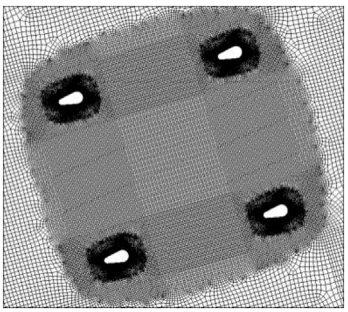

Fig. 3. Mesh near the ice-accreted 4-bundled conductor.

University of Tokyo and described in detail by Shimizu et al. (2004).

3.1. Verification of single-conductor models

Fig. 5 shows the variation of the aerodynamic coefficients with the angle of attack for a single conductor with $H = 1D$ for $L = 1D$ and $L = 10D$. Regarding C_D, the predicted results exhibit a flat response with an angle of attack in the range between 0° and 12°, followed by an increase as the angle of attack increases. The results of $L = 1D$ and $L = 10D$ show the same trends and are in good agreement with the wind tunnel test results. In the case of C_L, linear decreases are observed until an angle of attack of 12°; thereafter, the figure exhibits an acute increase at approximately 12°, followed by a steady decrease for angles greater than 20°. The absolute values for C_L when $L = 1D$ at 16° and 20° are overestimated, whereas significant improvement was observed for $L = 10D$. Regarding C_M, the figure shows a linear increase until 12°, followed by a decrease from the peak at approximately 12°; the value steadily increased for angles greater than 20°. These trends and values are in good agreement with the experiments.

The three-dimensional characteristics of the flow are studied to clarify the effects of the span length on the flow pattern. Fig. 6 shows the pressure contour at the angle of attack of 16° for $L = 1D$ and $L = 10D$. As shown in the figure, strong three-dimensionality is observed for $L = 10D$ in the pressure distributions because the wake significantly varies in the spanwise direction. In contrast, two-dimensional characteristics are observed for $L = 1D$ because the span length is short, which restricts the three-dimensional mixture of the flow in the wake.

Fig. 7 shows the variation of the mean surface-pressure coefficient distribution with span length for 16°. The pressure distribution for the

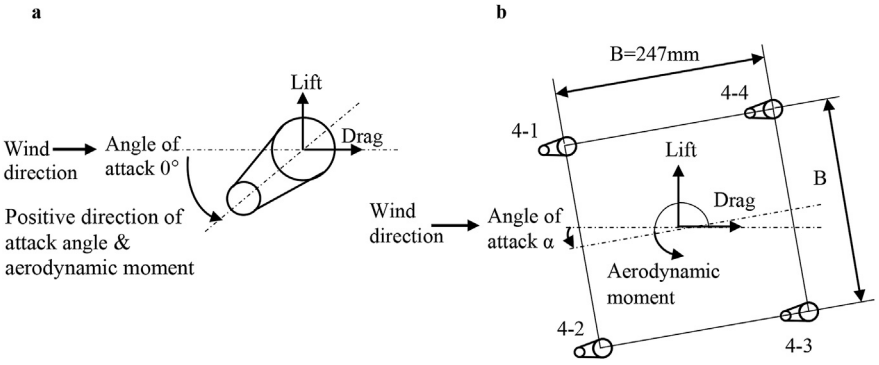

Fig. 4. Definition of the aerodynamic coefficients of (a) single conductor and (b) 4-bundled conductors.

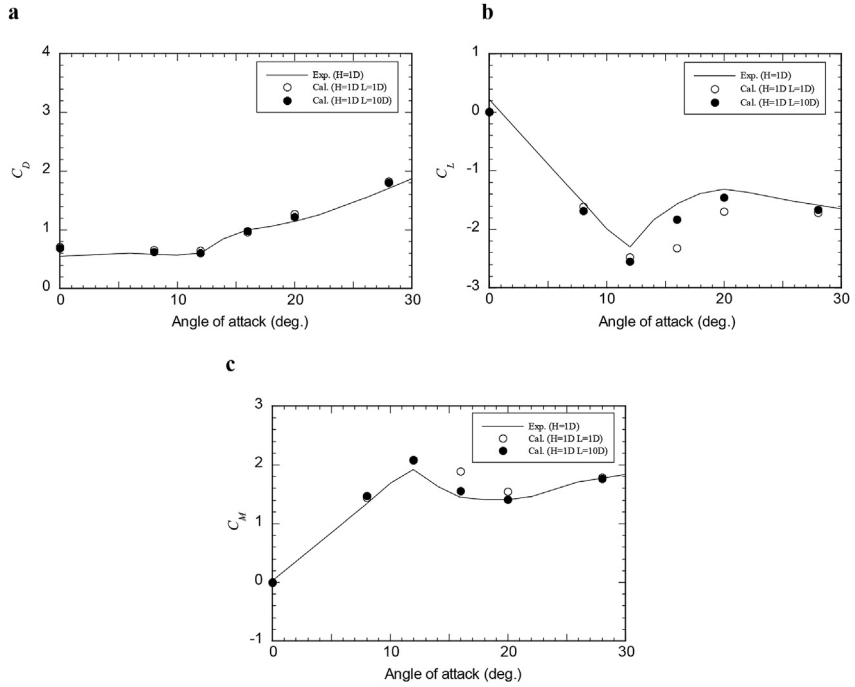

Fig. 5. Variation of the aerodynamic coefficients with the angle of attack for a single conductor with $H = 1D$. (Exp. and Cal. denote the measured and calculated values).

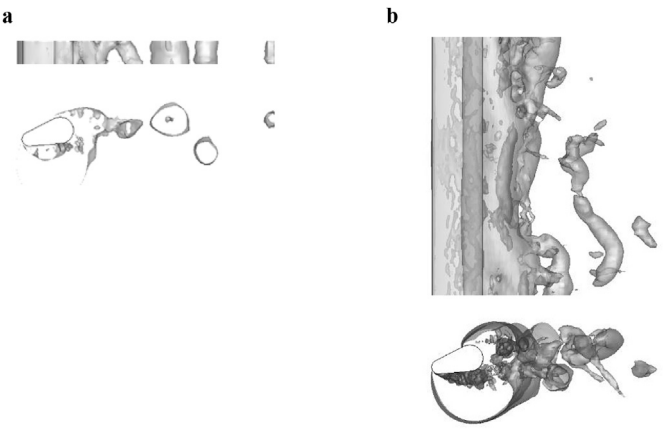

Fig. 6. Pressure contour at the angle of attack of 16°: (a) $L = 1D$ and (b) $L = 10D$.

region around the leading edge of the lower face ($X/D = 1.5$) of the conductor in the $L = 1D$ case exhibits strong negative pressure coefficients compared with the $L = 10D$ case, in which negative pressures are weakened due to the mixture of a large vortex in the wake. It is indicated that those differences in the pressure distributions cause the overestimation of the absolute value of C_L for $L = 1D$.

The spanwise length used in the wind tunnel test is $L = 90D$ (Shimizu et al., 2004), whereas $L = 10D$ is used in the analysis. Next, a systematic error estimation with the predicted results of three cases, $L = 2D$, $3D$, and $6D$, is conducted to validate whether $L = 10D$ is sufficiently long for this study. Here, a predicted aerodynamic coefficient with a span length of $L = \gamma D$ is defined as φ_γ, and the corresponding estimated error is ε_γ. The aerodynamic coefficient with a sufficiently long span length model, Φ, can be expressed using the following equation.

$$\Phi = \varphi_\gamma + \varepsilon_\gamma \tag{17}$$

Assuming that the predicted error monotonically decreases with an increase in span length, the error term can be described using an exponential function (Oka and Ishihara, 2009).

$$\varepsilon_\gamma = \beta e^{-c\gamma} \tag{18}$$

where γ is a positive integer other than 0. Values of γ = 2, 3, and 6 are used in this study. Coefficient β and decay factor c can be obtained using the following equation (Oka and Ishihara, 2009).

$$\beta = \frac{\phi_{\gamma+1} - \phi_\gamma}{1 - e^{-c}} e^{c\gamma}, \qquad c = \ln \frac{\phi_{\gamma+1} - \phi_\gamma}{\phi_{\gamma+2} - \phi_{\gamma+1}} \tag{19}$$

Fig. 8 shows the variation of the prediction error of the lift coefficients with span length at an angle of attack of 16°. The estimated error from the estimation error curve for $L = 10D$ is −0.02. The difference between the results of the computation for C_L with $L = 10D$ and the estimated value (1.84) is only 0.08%, which indicates that there is no dependency upon the span length; as a result, it can be concluded that $L = 10D$ is a sufficiently long length. However, as shown in Fig. 5(b), substantial differences are found between the results of the wind tunnel test and the values for C_L obtained by the numerical analysis for $L = 10D$. The reason for this difference is explained as follows. In general, it is impossible to create a perfectly symmetrical geometry model, which may lead to asymmetrical results of the wind tunnel test due to the asymmetrical geometry. For a curved surface, the flow separation point is not fixed, which causes an asymmetrical flow field, resulting in the aerodynamic coefficients becoming asymmetrical. This behavior is observed in the results of the wind tunnel test.

C_L should be zero at an angle of attack of 0° if the model is completely symmetrical; however, the wind tunnel test results show that C_L at angle of attack 0° is 0.22. In contrast, the model in the numerical analysis are symmetrical, and C_L is almost zero at the angle of attack 0°. Table 2 shows the difference between the measured and predicted values for C_D, C_L and C_M. The difference between the predicted value and the experiments up to 16° is almost the same as the error (0.22) observed at 0° in the experiment. Therefore, it is estimated that the discrepancy between the predicted results and the experiments is caused by the imperfection of the wind tunnel test model rather than numerical errors.

3.2. Verification for a 4-bundled conductor transmission line

Fig. 9 shows the variation of the aerodynamic coefficients with the angle of attack for a 4-bundled conductor with $H = 1D$ plotted with the wind tunnel test results. From these figures, although the calculation results for C_M and C_D for the 4-bundled conductors are good agreement with the experimental results, the absolute values of C_L overestimated the experimental values for the range of 12°–20°. In the range between 12° and 20°, the C_L may be smoothed because the model of the wind tunnel test is not completely symmetrical.

Fig. 10 shows a comparison of the experimental values of the aerodynamic coefficients for the single conductor and the 4-bundled conductor, in which the aerodynamic coefficients for the 4-bundled conductor are estimated from that of both positive and negative sides attack angles of the single conductor. As expected, the C_L values of the 4-bundled conductor estimated from that of the single conductor from the positive and negative sides of attack angles do not match the experiment. However, the absolute values for C_L between 12° and 20° become smaller and approach the experimental values if the average of both C_L estimated from the positive and negative attack angles of the single conductor is taken. Each conductor model is assumed to be randomly asymmetrical, indicating that the peak values have smoothed out together with the cancelling out of the asymmetrical characteristics of the 4-bundled conductors. Thus, the discrepancy between C_L and C_M from the wind tunnel test and the predicted those for the 4-bundled conductors as shown in Fig. 9 (b) and (c) is regarded as the error caused by model imperfection of the wind tunnel test rather than by numerical error.

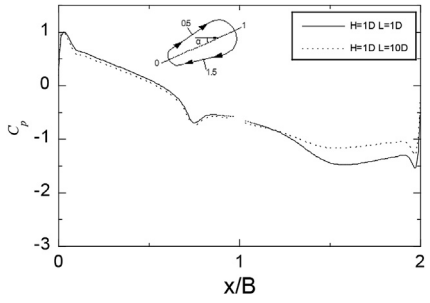

Fig. 7. Variation of the distribution of the mean surface pressure coefficients with span length.

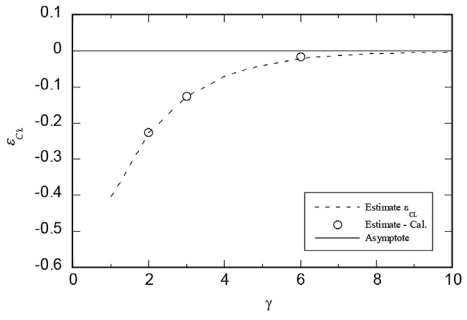

Fig. 8. Variation of the prediction error of the lift coefficients with span length at the angle of attack of 16°.

Table 2
Difference between the measured and predicted values shown in Fig. 5 for the cases with L = 10D.

Angle of attack °	0	8	12	16	20	28
ΔC_D	0.13	0.04	0.00	0.02	0.06	0.10
ΔC_L	0.22	0.14	0.25	0.28	0.15	0.08
ΔC_M	0.03	0.13	0.17	0.10	0.00	0.02

4. Aerodynamic characteristics of ice accreted transmission lines

In this section, the aerodynamic coefficients with regard to the variation in the height of the accreted ice for the single conductor transmission line are investigated. Next, the results of the numerical analysis and the wind tunnel test are compared to identify the flow mechanism according to the pressure distribution around the conductors. Subsequently, we obtain the aerodynamic coefficients for each conductor using numerical analysis, investigate the wake effects of the windward conductors on the leeward conductors, and then identify its mechanism from the pressure distribution around the conductors. Finally, a correction coefficient for aerodynamic coefficients of 4-bundled conductors from that of the single conductor is proposed to account for the wake effect of the windward conductors.

4.1. Variation in the aerodynamic coefficients with respect to the height of the accreted ice

Fig. 11 shows the variation of the aerodynamic coefficients with the angles of attack for single conductors with $H = 0.25D$, $0.5D$ and $1D$.

C_D is almost constant for $H = 0.25D$. In contrast, C_D is almost flat between 0° and 12° for $H = 0.5D$, after which it decreases from approximately 14° and then increases again from approximately 18°. C_D is smallest in the range between 0° and 12° for $H = 1D$ and then increases for angles greater than 12°. Although the results from the numerical analysis are slightly overestimated for $H = 0.25D$, the predicted results successfully reproduce the wind tunnel test results for $H = 0.5D$ and $H = 1D$.

C_L steadily decreases with increasing angles of attack for $H = 0.25D$. In contrast, for $H = 0.5D$, C_L decreases from 0°, peaks at 18°, rapidly recovers at approximately 20°, and then remains nearly constant for higher angles of attack. The value of C_L peaks at approximately 12° for $H = 1D$. All of those cases show that the numerical analysis results are close to the wind tunnel test results. The absolute values of C_L become smaller as the height of the accreted ice is increased at approximately 12°, whereas the absolute value of C_L decreases in the order of $H = 0.5D$, $1D$, and $0.25D$ at 16°, which is in good agreement with the results of the wind tunnel test.

Regarding C_M, the predicted results are in good agreement with that of the wind tunnel tests. C_M increases with the increase in the height of the accreted ice.

Fig. 12 shows the variation of the mean pressure distributions with the height of the accreted ice at angles of attack of 12° and 16°. At 12°, strong negative pressure is observed at the leading edge of the lower face where the height of accreted ice is $H = 1D$, which is consistent with the largest absolute value of C_L. In contrast, at 16°, the negative pressure is weakened around the leading edge of the lower face of the conductor for $H = 1D$, and the largest negative pressure is observed around the leading edge of the lower face for $H = 0.5D$, which also corresponds to the maximum absolute value of C_L. The strongest negative pressure is

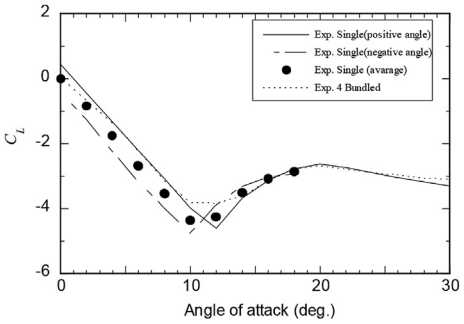

Fig. 10. Comparison of the aerodynamic coefficients from experimental values for the single conductor and the 4-bundled conductor.

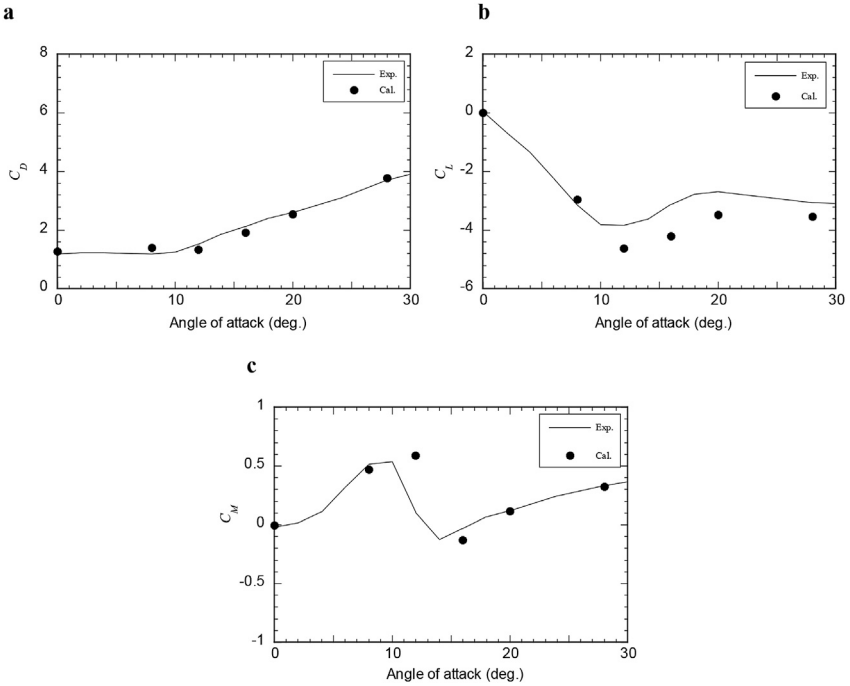

Fig. 9. Variation of the aerodynamic coefficients with the angle of attack for a 4-bundled conductor with $H = 1D$: (a) Drag coefficient, (b) Lift coefficient, and (c) Moment coefficient.

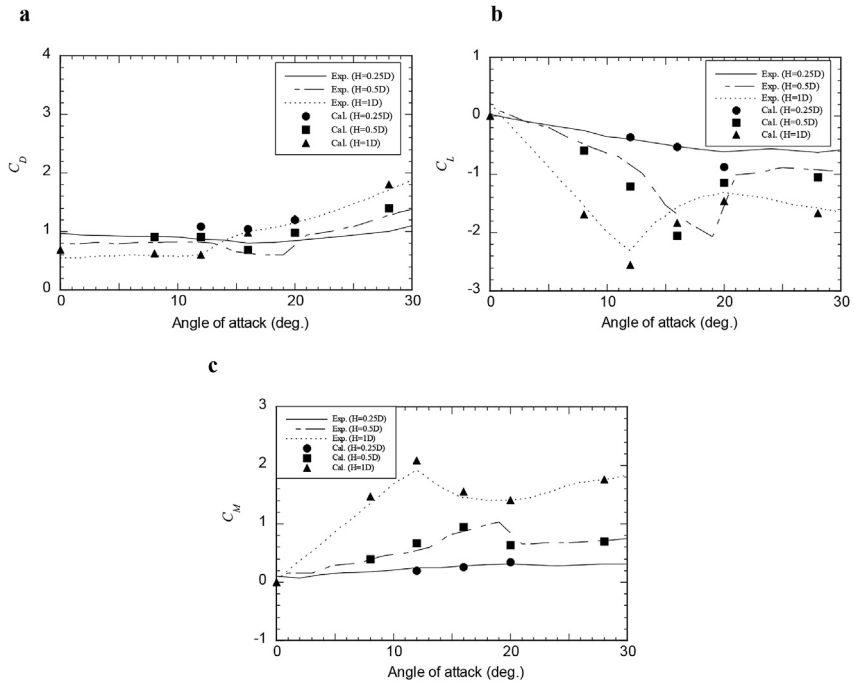

Fig. 11. Variation of the aerodynamic coefficients with angles of attack for single conductors with $H = 0.25D$, $0.5D$ and $1D$: (a) Drag coefficient, (b) Lift coefficient, and (c) Moment coefficients.

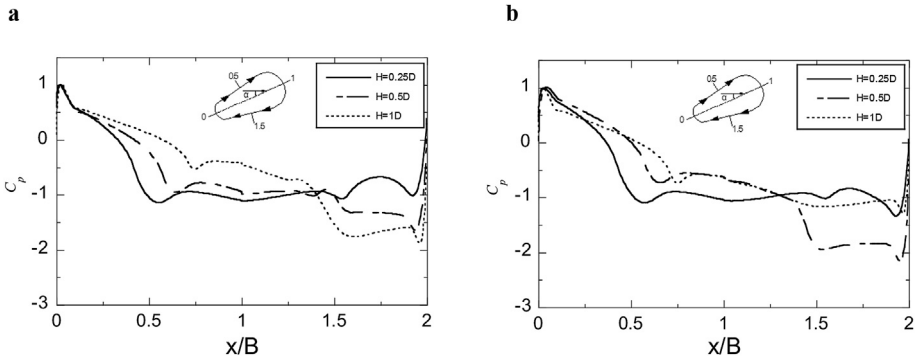

Fig. 12. Variation of the mean pressure distributions with the height of the accreted ice at angles of attack of (a) 12° and (b) 16°.

observed on the upper face of the conductor for $H = 0.25D$, where the vortex is reattached to the conductors.

4.2. Wake effects of the windward conductors

Shimizu et al. (2004) presented a method for converting the aerodynamic coefficients for 4-bundled conductors from that of a single conductor; however, no wake effect of the conductors was taken into account. In this study, the wake effects of windward sub-conductors are investigated. Fig. 13 shows a comparison of the aerodynamic coefficients for each sub-conductor plotted with the single-conductor results. At angles of attack of 8° and 12°, the values of C_L for the windward conductors (4-1 and 4-2) are small compared to those for the leeward conductors (4-3 and 4-4), while the values of C_L for the leeward conductors (4-3 and 4-4) are conversely decreased at 16°.

Fig. 14 shows the mean pressure distribution of each conductor at angles of attack of 12° and 16°. At 12°, strong negative pressure around the leading edge of the lower face of the windward conductors is observed in comparison to the leeward conductors, indicating that the wind speed decreased in this region because the wake of the windward conductors has reached the area in the vicinity of the leeward conductors. In contrast, at 16°, strong negative pressure around the leading edge of the lower face of the leeward conductors is observed compared with the pressure on the lower face of the windward conductors, which indicates that the downstream sub-conductors are located in the wind speed acceleration region because of the wake of the windward conductors.

The results of Shimizu et al. (2004) show that there are no large differences between the aerodynamic coefficient of 4-bundled conductors obtained from the single-conductor aerodynamic coefficients and those of 4-bundled conductors for C_D and C_L, while a discrepancy is observed in C_M, which implies that the wake has a strong impact on C_M. In this study, a correction coefficient, k, is proposed to account for the wake effect of the windward conductors, as shown in the modified formulas (20), (21), and (22) for C_D, C_L, and C_M, respectively.

$$C_D^4 = \frac{1}{2}\left\{C_D^{4-1} + C_D^{4-2} + k\left(C_D^{4-3} + C_D^{4-4}\right)\right\} \tag{20}$$

$$C_L^4 = \frac{1}{2}\left\{C_L^{4-1} + C_L^{4-2} + k\left(C_L^{4-3} + C_L^{4-4}\right)\right\} \tag{21}$$

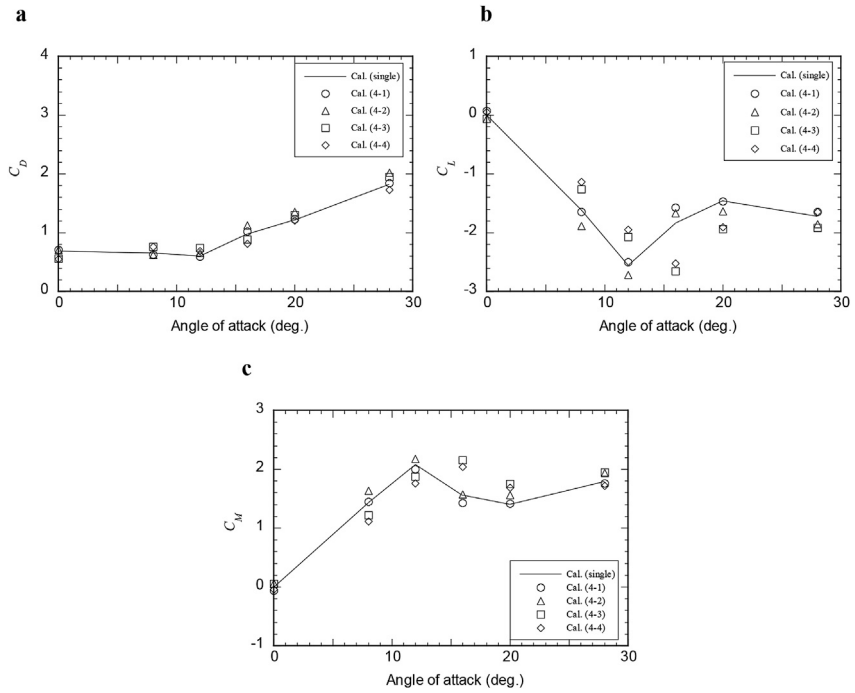

Fig. 13. Comparison of the aerodynamic coefficients for each conductor: (a) Drag coefficient, (b) Lift coefficient, and (c) Moment coefficients.

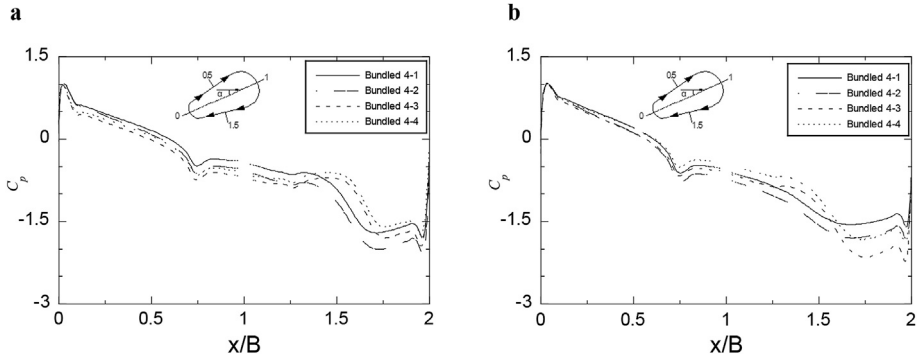

Fig. 14. Mean pressure distribution for each conductor: (a) angle of attack of 12° and (b) angle of attack of 16°.

$$C_M^4 = \frac{1}{2B}\{C_M^{4-1} + C_M^{4-2} + k(C_M^{4-3} + C_M^{4-4})\} + \frac{1}{2\sqrt{2}}(-C_D^{4-1} + C_L^{4-2} + k(C_D^{4-3} + C_L^{4-4}))\sin\left(\frac{\pi}{4} - \alpha\right) + \frac{1}{2\sqrt{2}}(-C_L^{4-1} + C_D^{4-2} + k(C_L^{4-3} + C_D^{4-4}))\cos\left(\frac{\pi}{4} - \alpha\right) \quad (22)$$

where k is obtained from the predicted C_M of the 4-bundled conductor. Note that at an angle of attack of 0°, k is obtained from the predicted C_D because C_L and C_M are zero.

Fig. 15 shows the variation of the correction coefficient k with respect to angles of attack ($H = 1D$). As shown in the figure, k is less than one in the range between 0° and 10°; k increases with the increase in the angles of attack for angles greater than 10° until it peaks at 16° and then decreases with an increase in the angle of attack.

Fig. 16 shows a comparison of the predicted aerodynamic coefficients of the 4-bundled conductors obtained from the single conductor with corrections and those obtained directly from the simulation for the 4-bundled conductor. The aerodynamic coefficients obtained using the correction coefficient k are in good agreement with the computed results for the 4-bundled conductors, thereby verifying the correction method.

5. Conclusions

The aerodynamic characteristics of single and 4-bundled ice-accreted transmission lines are investigated using the LES turbulence model and the following conclusions are obtained.

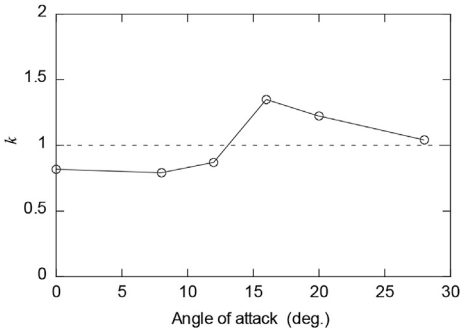

Fig. 15. Variation of the correction coefficient k with respect to the angle of attack ($H = 1D$).

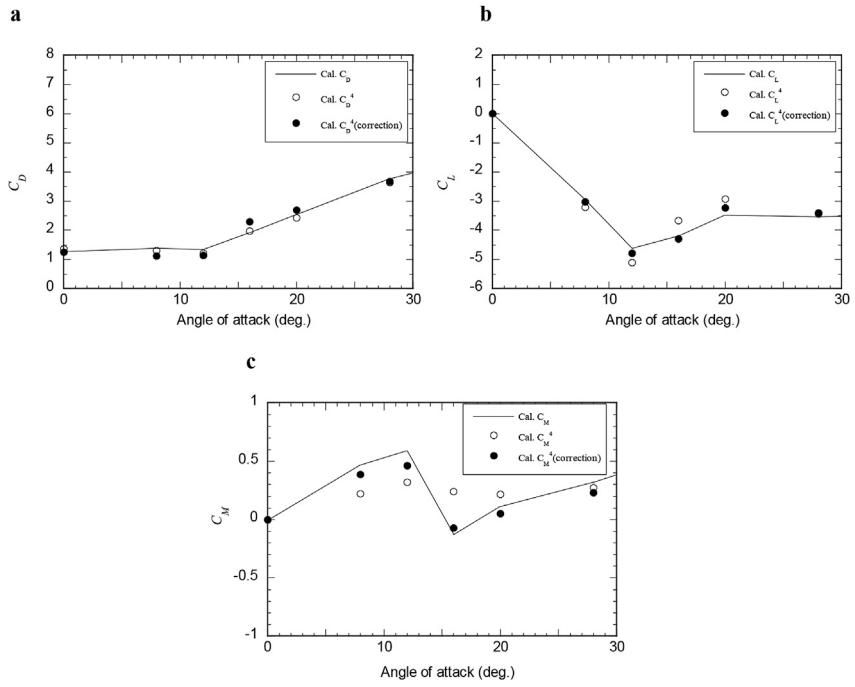

Fig. 16. Comparison of the aerodynamic coefficient obtained from a single conductor with corrections and that obtained directly from the 4-bundled conductor: (a) Drag coefficient, (b) Lift coefficient, and (c) Moment coefficients.

1. Accuracy verification tests for $L = 1D$ and $10D$ of the single conductor model show that C_L from the $L = 10D$ model improves the overestimation observed for $L = 1D$ at angles of attack of 16° and 20°, which is in good agreement with the wind tunnel test results.
2. The results of the systematic error estimation of the aerodynamic coefficients based on the models with $L = 2D$, $3D$, and $6D$ show that the span length $L = 10D$ is long enough to predict the aerodynamic coefficients. The discrepancy between the measurements and the predicted results for the $L = 10D$ model is found to be due to the wind tunnel test model imperfection rather than numerical error.
3. The impact of the height of the accreted ice on the aerodynamic coefficients and the pressure distribution around the conductors are investigated. It was found that the negative pressure around the leading edge of the lower face strongly affects C_L and C_M; in particular, the negative pressure is strong at 12° for $H = 1D$ and 16° for $H = 0.5D$, which correspond to the maximum absolute values of C_L and C_M, respectively.
4. The pressure distribution and the aerodynamic coefficients for each conductor are studied to identify the wake effects of the 4-bundled conductor. It was found that the wake of the windward conductors have a small influence on C_D of the leeward conductors, while it has a strong impact on both C_L and C_M. In addition, a proposed correction method related to the leeward conductors shows that the aerodynamic coefficients of the 4-bundled conductors converted from the single-conductor aerodynamic coefficients are in good agreement with the numerical analysis results of the 4-bundled conductors.

References

Cooper, K.R., 1973. Wind Tunnel and Theoretical Investigation into the Aerodynamic Stability of Smooth and Stranded Twin Bundled Power Conductors. National aeronautical establishment. Report LTR-LA-115.
Den Hartog, J.P., 1956. Mechanical Vibrations. McGrawHill.
Ferziger, J., Peric, M., 2002. Computational Method for Fluid Dynamics, third ed. Springer, Berlin.
Holmes, J.D., 2001. Wind Loading of Structures. Taylor & Francis, p. 117.
Kimura, K., Inoue, M., Fujino, Y., Yukino, T., Inoue, H., Morishima, H., 1999. Unsteady forces on an ice-accreted four-conductor bundle transmission line. In: Proceedings of 10th International Conference on Wind Engineering (ICWE10), pp. 467–472.
Matsumiya, H., Shimizu, M., Nishihara, T., 2010. Steady aerodynamic characteristics of single and four-bundled conductor transmission line with ice accretion. J. Struct. Eng. 56A, 588–601 (in Japanese).
Matsumiya, H., Nishihara, T., 2012. Wind tunnel tests for simulating large-amplitude, low-frequency galloping on overhead transmission lines. In: Proceedings of 7th International Colloquium on Bluff Body Aerodynamics and Applications (BBAA7), pp. 715–724.
Matsumiya, H., Nishihara, T., 2013. Study on aerodynamic force model of large-amplitude galloping of four-bundled conductors. Wind Eng., JAWE 38 (4), 87–100 (in Japanese).
Novak, M., 1972. Galloping oscillations of prismatic structure. Proc. ASCE 98. No. EM1.
Oka, S., Ishihara, T., 2009. Numerical study of aerodynamic characteristics of a square prism in a uniform flow. J. Wind Eng. Ind. Aerod. 97, 548–559.
Oka, S., Ishihara, T., 2010. Numerical study on steady aerodynamic characteristics of ice accreted transmission lines. In: Proc. 5th CWE2010, pp. 23–27.
Parkinson, G.V., 1971. Wind-induced instability of structure. Phil. Trans. Roy. Soc. Lond. 269, 395–409.
Rodi, W., 1997. Comparison of LES and RANS calculations of the flow around bluff bodies. J. Wind Eng. Ind. Aerod. 69–71, 55–75.
Scanlan, R.H., 1972. A Wind Tunnel Investigation of Bundled Power-line Conductors, Part VI, Observations on the Problem. NAE, NRC, Ottawa, Canada. Report No.LTR-LA-121.
Shimizu, M., Sato, J., 2001. Galloping observation and simulation of a 4-bundled conductor bundled transmission line. J. Struct. Eng. 47A, 479–488 (in Japanese).
Shimizu, M., Ishihara, T., Phuc, P.V., 2004. A wind tunnel study on aerodynamic characteristics of ice accreted transmission lines. In: Proc. Of BBAA V, pp. 369–372.
Smagorinsky, J., 1963. General circulation experiments with the primitive equations. I. The basic experiment. Mon. Weather Rev. 91, 99–164.